Effect of dynamical deformation on the production distribution in multinucleon transfer reactions

Shu Qing Guo,[1,2] Xiao Jun Bao,[3] Hong Fei Zhang,[4] Jun Qing Li,[4,5] and Nan Wang[1,*]

[1]*College of Physics and Energy, Shenzhen University, Shenzhen 518060, China*

[2]*Key Laboratory of Optoelectronic Devices and Systems of Ministry of Education and Guangdong Province, College of Optoelectronic Engineering, Shenzhen University, Shenzhen 518060, China*

[3]*Department of Physics, Hunan Normal University, Changsha 410081, China*

[4]*School of Nuclear Science and Technology, Lanzhou University, Lanzhou 730000, China*

[5]*Institute of Modern Physics, Chinese Academy of Sciences, Lanzhou 730000, China*

(Received 11 September 2019; published 19 November 2019)

Effects of dynamical deformation on the potential energy surface and the mass distribution in multinucleon transfer (MNT) reactions ^{136}Xe + ^{208}Pb, ^{136}Xe + ^{198}Pt are studied in the framework of the dinuclear system concept. Considering the dynamical deformation rather than the ground-state deformation of the two interacting nuclei, the products distribution could be estimated in agreement with experimental data, especially in the region far from the incident channel. On this basis, the orientation effect on the final isotopic production is discussed. The present calculation supports the tendency of the MNT reaction to maintain a larger production of neutron-rich isotones around $N = 126$, compared with the fragmentation reaction.

DOI: 10.1103/PhysRevC.100.054616

I. INTRODUCTION

The production of very neutron-rich and superheavy nuclides has aroused great interest not only in studying their structural properties and decay mechanism, but also in understanding the important processes of astrophysics and the formation of elements heavier than iron in the stellar evolution process [1–3]. In the experiment, many laboratories, such as GSI [4,5], Dubna [6,7], Argonne [8], GANIL [9], have performed various research works and made great achievements in producing these new nuclides of interest. However, many difficulties have been encountered since the low production cross sections and the great challenge of separation and isotopic identification [4]. Theoretical study on the mechanism of the diffusion process in heavy-ion collisions is of crucial importance, where one of the most important purposes is to provide optimal experimental conditions for the production of neutron-rich or superheavy nuclei of interest, such as the optimal projectile-target combination and the optimal incident energy.

In a recent review [10], experimental cross sections for several nucleon transfers are found to be relatively large, even at an incident energy close to the Coulomb barrier. Then the renewed interest in the multinucleon transfer (MNT) reaction at incident energies near the Coulomb barrier attracts great attention to populate neutron-rich nuclei in the region of the neutron shell closure $N = 126$ [6]. In this case, the primary product of the MNT reaction may share a low excitation energy, leading to an opportunity to survive against fission and to stay neutron-rich after the de-excitation process via neutron emission. The advantage of MNT reaction becomes more and more striking when producing neutron-rich nuclei in a heavy region and opens a possibility to study the structure and decay property of nuclei far from the β stability line [11–14].

Theoretical studies of the MNT reaction have been carried out based on both the semiclassic models, such as the GRAZING model [15–17], the Langevin-type approach [18–21], the dinuclear system (DNS) model [22–28], and the Complex WKB [29,30], and the microscopic methods, like the time-dependent Hartree-Fock (TDHF) [31–36], the improved quantum molecular dynamics (ImQMD) [37–40], and the stochastic mean-field approach [41–46]. Factors, such as the mass asymmetry of projectile-target combination [47,48], the shell structure [49–51], the isospin diffusion [52–55], the deformation and corresponding orientation effects [25,56], which influence the diffusion process from the contacting configuration to the separation, have also been studied in many works. However, not very much work involves the dynamical deformation in the diffusion system [20,21].

During the MNT reaction, the system is heated by the dissipation of the radial kinetic energy, and the excited nucleons can be distributed at many different energy levels. The position change of such nucleons results in an irreversible deformation, and the excitation energy deposits in the deformation degree of freedom [57]. Deformations of the reaction partners are not the ground-state ones any more [20,21,54,55,57]. Thus the internal structure of the colliding nuclei have to change to have different masses. The change will alter the interaction, and again the internal structure of the colliding nuclei will change due to the altered interaction. So that the relative motion is coupled with the nuclear intrinsic motion. Owing to the coupling between the collective and intrinsic variables and the

*wangnan@szu.edu.cn

coupling between the relative motion and the nuclear intrinsic motion mentioned above, it should be possible to predict that at the beginning of the collision, the shape of the system is dominated by the corresponding ground-state deformations of the two interacting nuclei, but as the diffusion proceeds, the shape of the system may change smoothly. Time-dependent deformation instead of ground state deformation or sphere should be expected to describe the diffusion process of the system.

In the framework of the DNS concept, the MNT reaction can be regarded as a process of massive nucleon transfer between the two colliding nuclei, with the relative kinetic energy being dissipated into the intrinsic excitation energy and the deformation being coupled with nucleon transfer. The advantage of the DNS in describing the system diffusion is that the dynamical deformations of the two interacting nuclei can be regarded as dynamical variables, which can allow a better understanding of behaviors of the time-dependent multidimensional potential energy surface (PES), shedding some interesting light on the reaction mechanism.

II. THEORETICAL FRAMEWORK

A. DNS model with dynamical deformation

Because of a strong Coulomb and nuclear interaction of the two heavy interacting nuclei, deformations of the reaction partners are no longer the ground-state ones. Dynamical deformation is expected to be considered in the process of the evolution from the contacting of the colliding nuclei to the separation of projectile-like and target-like products or to the fusion [20]. The DNS configuration $(Z_1, N_1, \beta_1, \beta_2)$ can be described by four macroscopic variables, namely, the proton number, neutron number, and deformations of two interacting nuclei. The evolution of the system is described by the following four-dimension master equation [58]:

$$\begin{aligned}\frac{dP(Z_1,N_1,\beta_1,\beta_2,t)}{dt} &= \sum_{Z_1'} W_{Z_1,N_1,\beta_1,\beta_2;Z_1'}(t)[d_{Z_1,N_1,\beta_1,\beta_2}P(Z_1',N_1,\beta_1,\beta_2,t) \\ &\quad - d_{Z_1',N_1,\beta_1,\beta_2}P(Z_1,N_1,\beta_1,\beta_2,t)] \\ &\quad + \sum_{N_1'} W_{Z_1,N_1,\beta_1,\beta_2;N_1'}(t)[d_{Z_1,N_1,\beta_1,\beta_2}P(Z_1,N_1',\beta_1,\beta_2,t) \\ &\quad - d_{Z_1,N_1',\beta_1,\beta_2}P(Z_1,N_1,\beta_1,\beta_2,t)] \\ &\quad + \sum_{\beta_1'} W_{Z_1,N_1,\beta_1,\beta_2;\beta_1'}(t)[d_{Z_1,N_1,\beta_1,\beta_2}P(Z_1,N_1,\beta_1',\beta_2,t) \\ &\quad - d_{Z_1,N_1,\beta_1',\beta_2}P(Z_1,N_1,\beta_1,\beta_2,t)] \\ &\quad + \sum_{\beta_2'} W_{Z_1,N_1,\beta_1,\beta_2;\beta_2'}(t)[d_{Z_1,N_1,\beta_1,\beta_2}P(Z_1,N_1,\beta_1,\beta_2',t) \\ &\quad - d_{Z_1,N_1,\beta_1,\beta_2'}P(Z_1,N_1,\beta_1,\beta_2,t)], \end{aligned} \tag{1}$$

where the $P(Z_1, N_1, \beta_1, \beta_2, t)$ denotes the probability distribution to find fragment 1 with Z_1, N_1, with deformations β_1, β_2 (here, only the most important axially symmetric quadrupole deformations are considered, and always the tip-to-tip orientation is taken; unless the orientation effect is discussed later), with local excitation energy E_J^* at time t, with the incident angular momentum J. β_1, β_2 are taken as two discrete macroscopic variables. $W_{Z_1,N_1,\beta_1,\beta_2;Z_1'}$ is the mean transition probability from the channel $(Z_1, N_1, \beta_1, \beta_2)$ to the channel $(Z_1', N_1, \beta_1, \beta_2)$. $d_{Z_1,N_1,\beta_1,\beta_2}$ represents the microscopic dimension of the corresponding macroscopic state $(Z_1, N_1, \beta_1, \beta_2)$. The initial condition corresponds to the incident channel. The interaction time, which is dependent on the incident energy and incident angular momentum in the dissipative process, could be determined by using the classic deflection function method [59–61]. See Refs. [27,28,62] for more details.

In the relaxation process of relative motion, the DNS heated by the local excitation energy opens a valence space $\Delta\varepsilon$, which has a symmetrical distribution around the Fermi surface. Only the particles in the states within this valence space are actively involved in the excitation and transfer [63]. With the mean single-particle densities g_1, g_2, we have the valence states $N_1 = g_1\Delta\varepsilon$, $N_2 = g_2\Delta\varepsilon$ and corresponding valence nucleons $m_1 = N_1/2$, $m_2 = N_2/2$. $\Delta\varepsilon$ is related to the local excitation energy by $\Delta\varepsilon = \sqrt{4E_J^*/g}$, with $g = (g_1 + g_2)/2$ and g_k being approximately from $A_k/8$ to $A_k/16$ [63,64]. The quantity E_J^* denotes the local excitation energy of the DNS configuration with incident angular momentum J, which is defined as $E_J^* = E_x(J,t) - [U(Z_1, N_1, \beta_1, \beta_2, J) - U(Z_P, N_P, \beta_P, \beta_T, J)]$. The first term, $E_x(J,t)$, is the radial dissipation energy, which is related to the Coulomb barrier and is determined for each initial relative angular momentum J by the parametrization method of the classical deflection function [59–61].

The four macroscopic collective variables mentioned above determine the PES of the DNS:

$$\begin{aligned}U(Z_1,N_1,\beta_1,\beta_2,J) &= E(Z_1,N_1,\beta_1) + E(Z_2,N_2,\beta_2) \\ &\quad + V_{\rm CN}(Z_1,N_1,\beta_1,\beta_2,R_{\rm cont}) \\ &\quad + V_{\rm rot}(Z_1,N_1,\beta_1,\beta_2,R_{\rm cont},J), \end{aligned} \tag{2}$$

where quantity $E(Z_i, N_i, \beta_i)$ is the total energy of the ith nucleus of DNS as a function of shape given by the macroscopic-microscopic model, $E(Z_i, N_i, \beta_i) = E_{\rm LD}(Z_i, N_i)\prod_k(1 + b_k\beta_{ik}^2) + cE_{\rm sh}(Z_i, N_i, \beta_i)$ [65]. Here, only quadrupole deformation β_{i2} is considered, denoted with $\beta_i \equiv \beta_{i2}$. The nucleus-nucleus interaction potential energy $V_{\rm CN}$ between two interacting nuclei of the DNS configuration is the sum of Coulomb interaction potential $V_{\rm C}$ calculated by Wong's formula [66] and the nuclear interaction potential $V_{\rm N}$ obtained from the folding integral of a zero-range nucleon-nucleon interaction [67,68]. The rotational energy $V_{\rm rot} = \hbar^2 J(J+1)/\Im_{\rm tot}$, where the moment of inertia $\Im_{\rm tot}$ is approximated by its rigid-body value. Because of the disappearance of the Coulomb barrier for a sufficiently heavy system, the critical position where the nucleon transfer process takes places can be assumed by $R_{\rm cont} = R_1(1 + \beta_1 Y_{20}(\theta_1)) + R_2(1 + \beta_2 Y_{20}(\theta_2)) + 0.7$ fm, with $R_i = 1.16A_i^{1/3}$.

The isotope cross section of the primary fragment produced in the MNT reaction can be calculated by

$$\sigma_{\rm pri}(Z_1,N_1)=\frac{\pi\hbar^2}{2\mu E_{\rm c.m.}}\sum_J(2J+1)T(E_{\rm c.m.},J)\times\sum_{\beta_1,\beta_2}P(Z_1,N_1,\beta_1,\beta_2,J,\tau_{\rm int}),\quad(3)$$

where the penetration coefficient $T(E_{\rm c.m.},J)$ describes the probability of the colliding nuclei at the incident energy $E_{\rm c.m.}$ overcoming the interaction barrier in the entrance channel. It is assumed that when the incident energy is higher than the interaction barrier, $T(E_{\rm c.m.},J)$ is estimated to be 1, while to be 0 for other cases.

When the primary partners begin to separate, deformations of projectile-like and target-like fragments are no longer the ground-state ones at the exit channel. The total excitation energy of primary fragments can be expressed as $E_{\rm tot}=E_{\rm c.m.}-{\rm TKE}+Q_{gg}$, where Q_{gg} value corresponds to the reaction energy of the exit channel of interest, the total kinetic energy (TKE) of the outgoing $(Z_1,N_1,\beta_1,\beta_2)$ configuration is the sum of the Coulomb energy, nuclear energy, and radial kinetic energy at the exit [60]. The excitation of primary products shares the value of $E_{\rm tot}$ in proportion to their masses $E^*_{Z_1,N_1}=E_{\rm tot}\cdot A_1/(A_1+A_2)$, where A_1,A_2 are the corresponding mass number.

B. Production of final products

To obtain the characteristics of final products, the state-of-art statistical model code GEMINI++ is employed, which takes into account the evaporation of neutrons, protons, α particles, and γ quanta, as well as fission of an excited nucleus [69,70]. This model is an updated version of GEMINI based on the Monte Carlo simulation, which can well describe the fission decay width for heavy systems [71].

For a certain primary product $(Z_1',N_1',E^*_{Z_1',N_1'},J'_{Z_1',N_1'})$, the de-excitation process should be simulated many times due to the statistical nature of GEMINI++. After $M_{\rm trial}$ times Monte Carlo simulations, events with (Z_1,N_1) are counted, the number of such events is marked as $M(Z_1,N_1;Z_1',N_1',J')$. Then the decay probability from the primary product (Z_1',N_1',J') produced at the incident angular momentum J' to the final product (Z_1,N_1) can be estimated as $P(Z_1,N_1;Z_1',N_1',J')=M(Z_1,N_1;Z_1',N_1',J')/M_{\rm trial}$. Finally, the production cross section of final product (Z_1,N_1) can be given as [35]

$$\sigma_{\rm fin}(Z_1,N_1)=\sum_{Z_1',N_1',J'}\sigma_{\rm pri}(Z_1',N_1',J')\times P(Z_1,N_1;Z_1',N_1',J').\quad(4)$$

The direct consequence of introducing the deformation of fragments as dynamical variables is that one should treat the orientation between the two deformed interacting nuclei [62]. On one hand, the initial mutual orientation of the colliding nuclei mainly influences the maximal value of the kinetic energy loss and the interaction time; on the other hand, due to coupling of the internal and collective degrees of freedom, the thermal fluctuations of the orientation configuration at the exit channel may exist, which could result in a broad distribution of TKE and affect the de-excitation process [21].

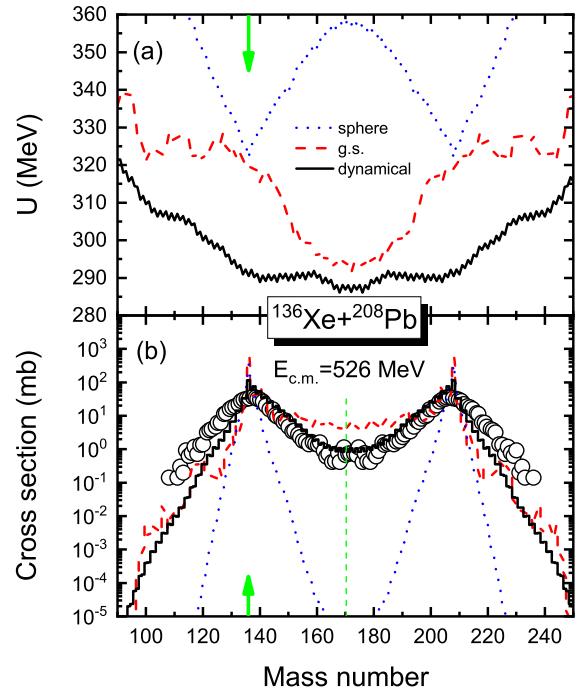

FIG. 1. (a) Potential energy surfaces of the ^{136}Xe + ^{208}Pb reaction $U(A_1)$, projected to the lowest potential energy valley of all possible configurations $(Z_1,N_1,\beta_1,\beta_2)$ at certain mass numbers A_1, are calculated with corresponding ground-state deformations (dashed red line), dynamical deformations (solid black line), and spheres (dotted blue line) of the two nuclei of the DNS. (b) Calculated mass distribution of primary products with bombarding energy $E_{\rm c.m.}=526$ MeV. The cross sections are obtained by the evolution of DNS with the three different deformation configurations. The arrow indicates the position of incident channel. Experimental data (circle) of primary products are taken from Ref. [6].

To simplify the calculation, it is usually assumed that the initial mutual orientation of interacting nuclei do not change in the whole diffusion process [7]. In the present work, two extreme conditions, tip-to-tip and side-to-side orientation configurations, are assumed to study the orientation effect on the diffusion and de-excitation processes. Another extreme assumption that the diffusion is governed by the PES of tip-to-tip configurations, but the separation is performed by side-to-side configurations at the exit point, is also discussed.

III. RESULTS AND DISCUSSIONS

A. Dynamical deformation

To assess the effect of dynamical deformation on PES and system evolution in the framework of the DNS concept, three different forms of deformations of nuclei of DNS configurations are assumed for discussion, as displayed in Fig. 1.

For the ^{136}Xe + ^{208}Pb reaction, the calculated PESs with ground-state deformation (dashed red line), dynamical deformation (solid black line), and sphere (dotted blue line) of DNS configurations are displayed in Fig. 1(a), respectively.

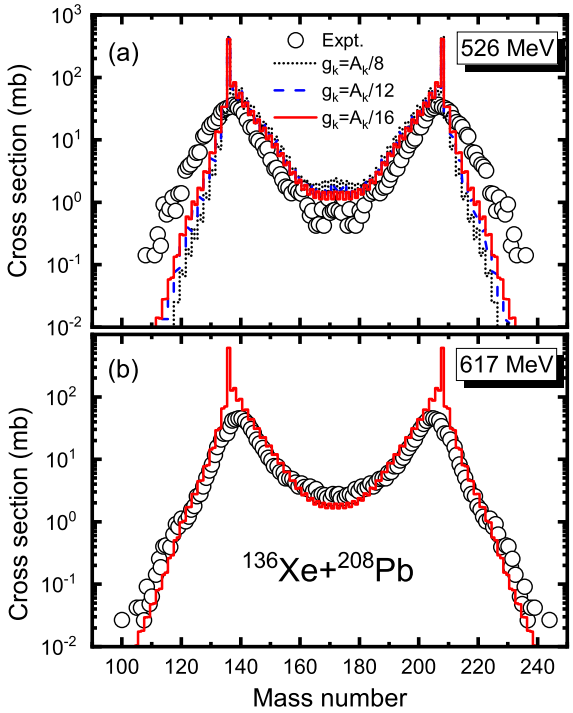

FIG. 2. (a) Mass distribution for primary products in the ^{136}Xe + ^{208}Pb reaction with bombarding energy $E_{\text{c.m.}} = 526$ MeV are calculated with different single-particle level density $g_k = A_k/8$ (dotted black), $A_k/12$ (dashed blue), and $A_k/16$ (solid red), respectively. (b) The same as above, but with $E_{\text{c.m.}} = 617$ MeV and $g_k = A_k/16$. The experimental data of primary products are taken from Ref. [6].

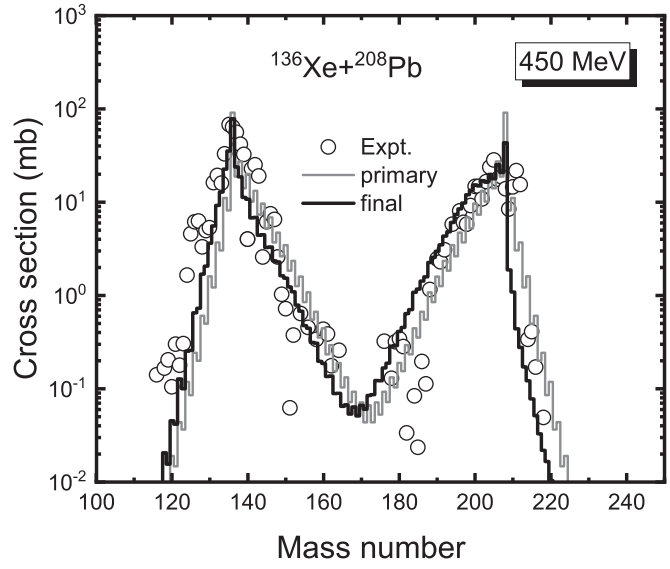

FIG. 3. Mass distribution for primary (light gray) and final (black) products in the reaction ^{136}Xe + ^{208}Pb with bombarding energy $E_{\text{c.m.}} = 450$ MeV. The experimental data of final products are taken from Ref. [8].

Figure 1(b) displays the calculated mass distributions of primary products governed by the three corresponding PESs with the bombarding energy $E_{\text{c.m.}} = 526$ MeV. The experimental cross sections of primary products are from Ref. [6], where most of the quasielastic events are excluded by recording events with TKE loss larger than 40 MeV. The present calculations do not exclude the above-mentioned events, overestimating the cross section only near the incident channel.

First, for the case of the ground-state deformation, shapes of nuclei (for example, in the region around $A_1 = 110$) may vary greatly, resulting in the landscape of the PES with large fluctuation, see Fig. 1(a) (dashed red line). Thus it is expected to predict that the corresponding mass distribution is very irregular. The cross section in the mass asymmetry region is underestimated, while in the mass symmetry region it is very overestimated, as shown (dashed red line) in Fig. 1(b). Second, the shape of the DNS configuration is dominated by the ground state deformation of the two interacting nuclei at the beginning of the collision, but may evolve into various macroscopic states of possible deformations with corresponding probabilities depending on excitation energies of the DNS configurations at different interaction time. From the behavior of the PES and mass production as shown (solid black line) in Fig. 1(a) and 1(b), it should be possible to predict that dynamical deformation is necessary to reasonably describe the evolution process and the relatively realistic mass distribution. Because of the influences of the very short contact time at the peripheral collision and the relative longer contact time at the damped collision, the calculated cross sections have similar shapes to the experimental data. Third, for comparison, by assuming that the spherical shape maintains throughout the evolution process, such PES leads to a relatively smooth but narrow distribution of primary products, as displayed (dotted blue line) in Fig. 1(a) and 1(b). Concerning the discussion mentioned above, dynamical deformation plays an important role in widening mass distribution in the MNT reaction.

B. Influence of collision energy

By considering the dynamical deformation, it can be supposed that $Z_1, N_1, \beta_1, \beta_2$ are the least number of macroscopic variables adequate for a complete specification of the macroscopic state of a DNS configuration. On the basis of present dynamical deformations, the calculation of mass distribution of primary products is relatively smooth and roughly consistent with the experimental data in the ^{136}Xe + ^{208}Pb reaction with bombarding energy $E_{\text{c.m.}} = 526$ MeV, see Fig. 2. The relatively small influence of uncertainty of the single-particle level densities on the nucleon transfer has been achieved as compared with assumed constants $g_k = A_k/8$, $A_k/12$, and $A_k/16$ in Fig. 2(a). To investigate the behavior of the MNT reaction at different collision energies, the calculated and experimental mass distributions for $E_{\text{c.m.}} = 526$ and 617 MeV are shown in Fig. 2(a) and 2(b), respectively. By comparing Fig. 2(a) and 2(b), it is found that the magnitude and the distribution width of primary products becomes larger with the increasing incident energy, keeping the shape of distribution almost unchanged. This remarkably indicates that higher excitation energy is beneficial to nucleon transfer. In addition, the low-lying distribution far from the incident channel goes up with the increasing energy, owing to contributions from

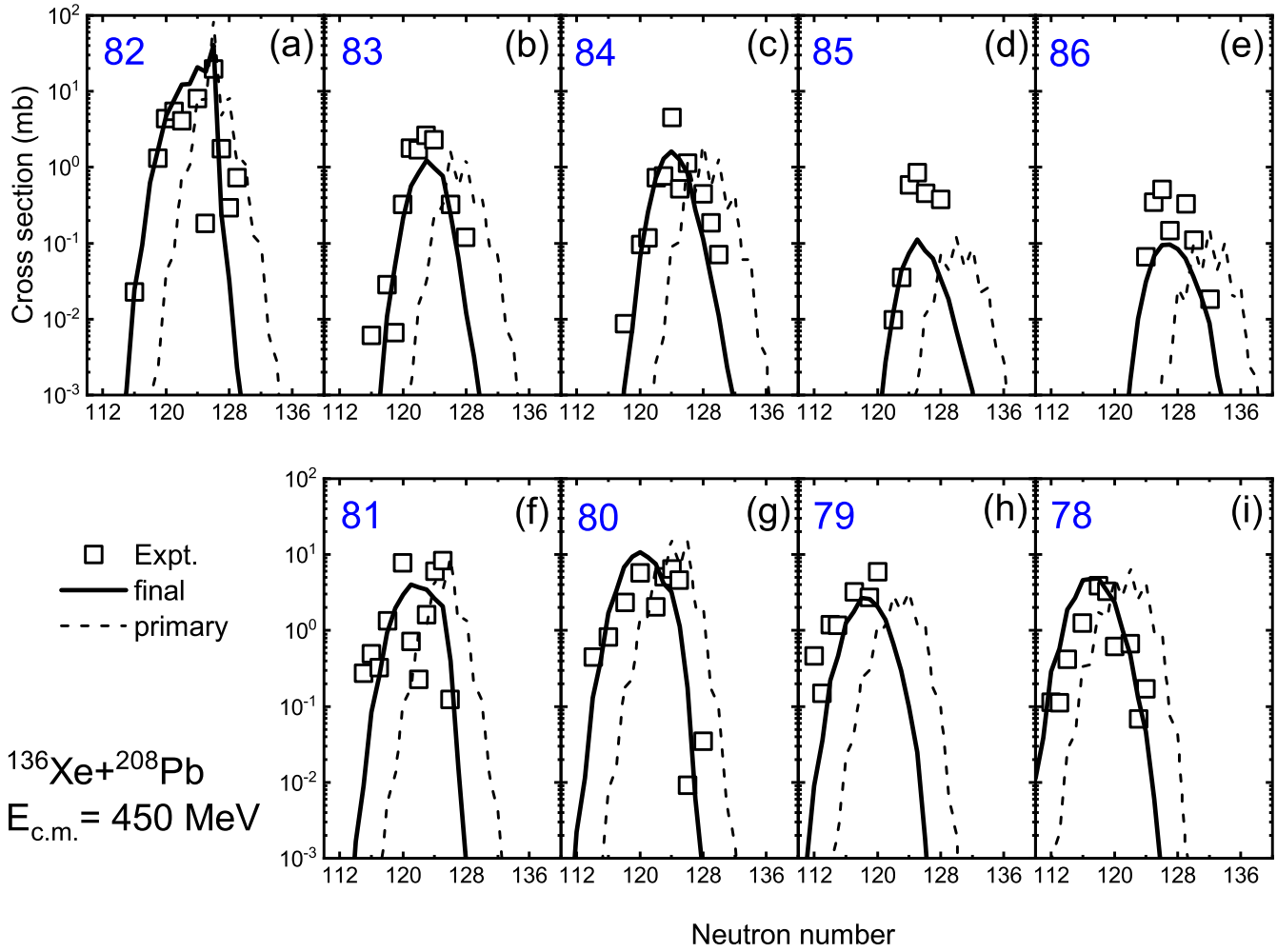

FIG. 4. Cross sections of isotopes of target-like fragments ($Z = 78$–86) in the $^{136}\mathrm{Xe} + {}^{208}\mathrm{Pb}$ reaction at bombarding energy $E_{\mathrm{c.m.}} = 450$ MeV. The primary and final products are denoted by the dashed and solid lines, respectively. The experimental data are taken from Ref. [8].

small impact parameters. The reasonable agreement between the calculated and experimental results of the mass distribution at different bombarding energies reveals the applicability of the DNS model to study the MNT reaction.

C. Primary and final products

In Fig. 3, the calculated cross sections of primary (light gray) products in the reaction $^{136}\mathrm{Xe} + {}^{208}\mathrm{Pb}$ with bombarding energy $E_{\mathrm{c.m.}} = 450$ MeV as a function of mass number are displayed. It can be seen that the mass distribution of primary products is symmetrical, which is due to the contributions from both the projectile-like and target-like products. The statical model GEMINI++ code is employed for the evaluation of final products. The calculated mass distribution of final products is well reproduced both on the position and the magnitude of the maximum, as shown by the black line in Fig. 3.

Careful observation of the primary and final product mass distribution in Fig. 3 reveals two such characteristics: the first one is that the shift of the mass distribution between primary and final products in the direction of mass reduction is small for lighter mass area but large in heavier mass area; the second one, the cross section of lighter final products at the corresponding maximum is larger than that of heavier ones, while the distribution width is opposite. It can be explained that under the assumption of thermal equilibrium at the exit, the heavier primary product shares a higher excitation energy, resulting in a significant reduction of neutrons after de-excitation, compared with the lighter one. The calculated mass distribution characteristics of the primary and final products are reasonably consistent with experiment, which provides a reliable tool for further study of the final isotope distribution of interest.

Based on the above discussion, we further estimate the isotopes distribution of interest. Figure 4 displays the comparison of the experimental and calculated target-like isotopic distributions from $Z = 78$ to 86 in the MNT reaction $^{136}\mathrm{Xe} + {}^{208}\mathrm{Pb}$ at bombarding energy $E_{\mathrm{c.m.}} = 450$ MeV. The primary and final products are denoted by dashed and solid lines, respectively. From the DNS calculation, it can be seen that a reasonable agreement with the experimental data has been

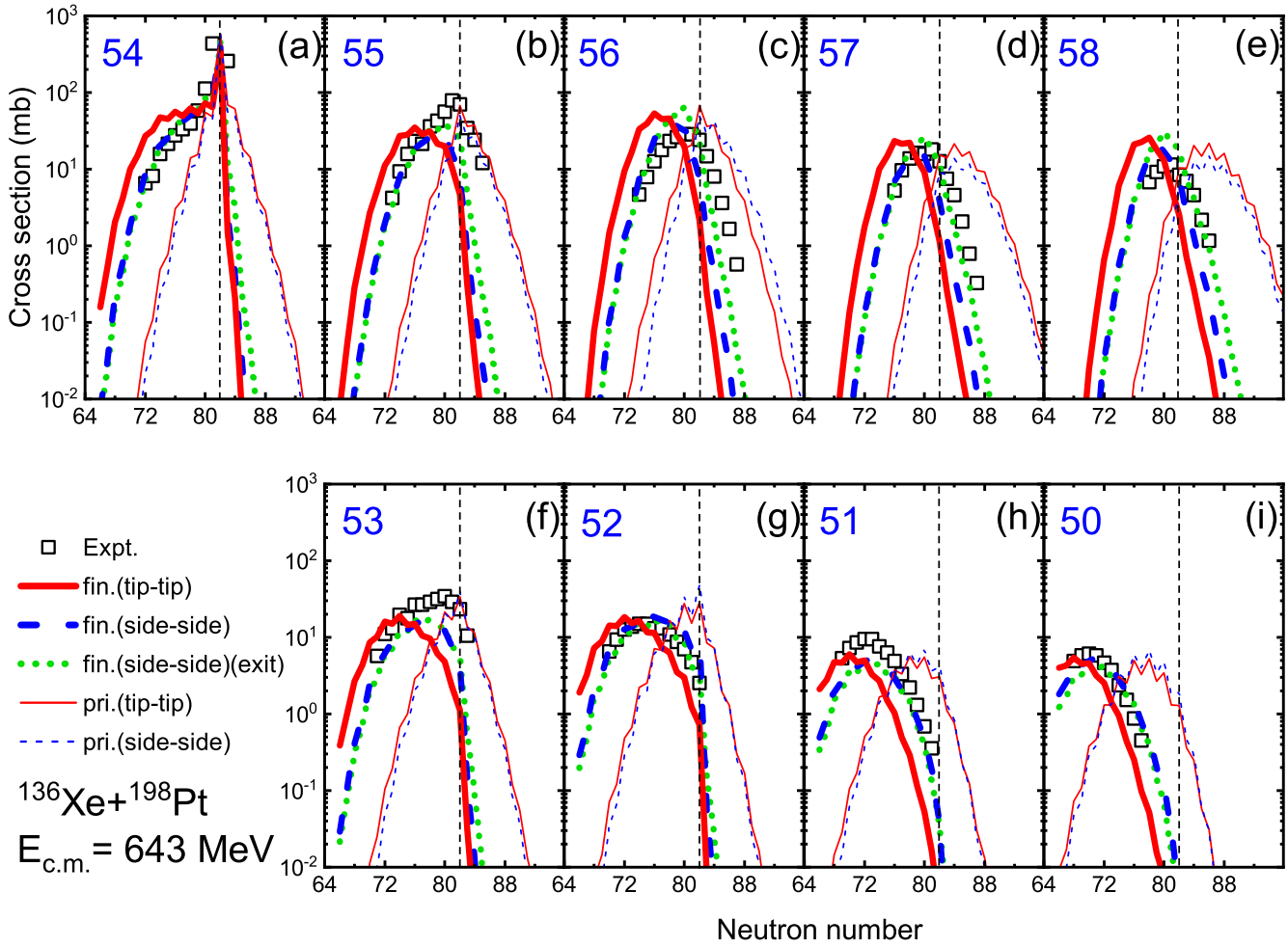

FIG. 5. Cross sections of final (thick lines) and primary (thin lines) projectile-like fragments ($Z = 50$–58) in the ^{136}Xe + ^{198}Pt reaction at bombarding energy $E_{\text{c.m.}} = 643$ MeV. Isotopes distributions are obtained through the evolution of the DNS governed by the PES of tip-to-tip (solid red) and side-to-side (dashed blue) configurations, respectively. The (dotted green) lines correspond to the results with the evolution process under the tip-to-tip orientation but with the separation under the side-to-side orientation. The experimental data of final products are taken from Ref. [9].

achieved by estimating the magnitude of cross sections and the location of peaks of the isotopic distributions, see Fig. 4.

To extend the conclusion of interest, Fig. 5 shows the measured isotopic distribution of different projectile-like products (from $Z = 50$ to 58) in the MNT reaction ^{136}Xe + ^{198}Pt at bombarding energy $E_{\text{c.m.}} = 643$ MeV, which is about 1.55 times the Coulomb barrier [9]. In their paper [9], Watanabe *et al.* reported a behavior of isotopic distribution that peak positions of the projectile-like products are moved with large shifts to lower mass number but small shifts to higher mass number as compared to the pure proton transfer channels, and this tendency becomes more striking for more proton transfer. Meanwhile, they suggest that the measured events could not directly correspond to the number of neutrons transferred, but correspond to the final products after neutron evaporation, in addition, neutron transfer is accompanied by proton transfer in the diffusion process.

However, by displaying the distribution as a function of the neutron number rather than the mass number, the above-measured behavior can be more clearly understood, as shown by open squares in Fig. 5. On the one hand, due to the nucleons transfer, the peak of the primary isotope distribution (thin solid red lines) for the proton pick-up channel ($Z > 54$) moves towards neutron increase ($N > 82$); on the other hand, the distribution moves towards neutron decrease by mainly evaporating neutrons from primary products. The final result is that the peak of the final isotope distribution (thick solid red lines) moves with a small amount of neutrons shift in the direction of neutron increase (or even decrease) relative to the position of the incident channel ($N = 82$), see Fig. 5(b)–5(e). Instead, for similar reasons, the peak of final products moves towards neutron increase for the proton stripping channel ($Z < 54$), but with a larger amount of neutrons shifts, see Fig. 5(f)–5(i). Similar behaviors are shown for ^{136}Xe + ^{198}Pt in Fig. 4.

It should be pointed out that the GRAZING model particularly well describes the isotopes distribution near the entrance channel, but underestimates the experimental value for large proton transfer, because it takes into account only a small range of impact parameters close to the GRAZING collision, see

Refs. [9,72] for a detailed discussion. However, in the present DNS calculation, not only the peripheral collision but also small impact parameter collisions are considered to contribute to the MNT products. The high energies dissipated from small impact parameter collisions help to transfer more nucleons but evaporate more neutrons, and the competition makes the calculated tendency of isotope distribution consistent with the experiment, as discussed above.

D. Orientation effect

In Fig. 5, we discuss the orientation effect on the final products distribution in ^{136}Xe + ^{198}Pt at bombarding energy $E_{\mathrm{c.m.}} = 643$ MeV. As mentioned above, for the case of the tip-to-tip configuration in the whole diffusion process, the final isotopes distribution (solid red) roughly reproduces most of the experimental data, especially in the trend, see Fig. 5. Nevertheless, the calculated primary products seems to evaporate too many neutrons, resulting in the final products being more neutron-deficient. The reason could be that the tip-to-tip configuration corresponds to the lower Coulomb barrier or TKE at the exit. Subtracting the ground state Q_{gg} value, the larger excitation energy makes the primary product evaporate more neutrons. However, other orientations corresponding to higher Coulomb barriers and lower dissipated energies could contribute to the production of final products by evaporating a small number of neutrons from primary products.

For the case of side-to-side orientation, the isotopic distributions from $Z = 50$ to 58 are obtained by the evolution of DNS suffering from the PES with side-to-side configurations, see Fig. 5 (dashed blue). It is found that the distributions move towards a neutron increase as compared with the tip-to-tip cases, which is in better agreement with the experiment. It can also be assumed that the evolution of the DNS is governed by a PES with tip-to-tip configurations, but the separation of primary products is described with side-to-side configurations at the exit point. The corresponding calculations are shown in Fig. 5 (dotted green). Similar behavior is obtained. The side-to-side orientation seems to favor the production of neutron-rich nuclei, since the large total kinetic energy is released at the exit channel.

To extend the products region of interest, calculated cross sections of all possible primary and final products produced in the ^{136}Xe + ^{198}Pt reaction with bombarding energy $E_{\mathrm{c.m.}} =$ 643 MeV are displayed in Fig. 6, respectively. It can be seen from Fig. 6(a) that primary products have considerable cross sections distributions with wide ranges in the chart nuclides. The MNT reaction is more likely to produce neutron-deficient nuclei especially in the vicinity of the incident, see wider peaks in Fig. 6(b) and 6(c). However, from characteristics of final isotope distributions around $N = 126$ obtained by tip-to-tip and side-to-side collision in Fig. 6(b) and 6(c), it is indicated that the side-to-side orientation has a greater advantage in producing neutron-rich nuclides as compared with the tip-to-tip one.

Figure 7 shows the comparison of isotones of $N = 126$ between the MNT reaction of ^{136}Xe + ^{198}Pb and the fragmentation reaction of ^{208}Pb(1 GeV/nucleon)+Be, respectively. The measurements show that isotones cross sections produced

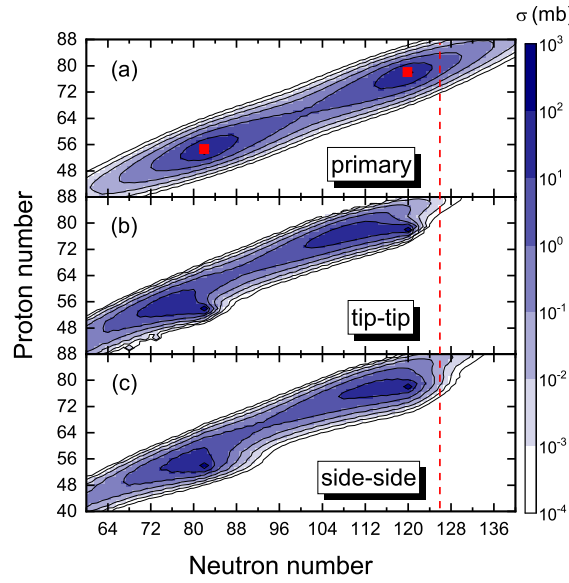

FIG. 6. (a) Calculated cross sections of primary products of isotopes produced in the ^{136}Xe + ^{198}Pt reaction with $E_{\mathrm{c.m.}} = 643$ MeV. (b) Calculated cross sections of final products after the de-excitation process where primary products are at higher excitation energies owing to the tip-to-tip configuration at the exit channel. (c) Same as (b) but for the side-to-side configuration at the exit channel. Red squares denote the positions of incident nuclei ^{136}Xe and ^{198}Pt. The dash line $N = 126$ is to guide the eyes.

from the MNT reaction is more than 2–3 orders of magnitude higher than those from the fragmentation reaction for producing very neutron-rich nuclei $Z < 77$. The present calculated distribution of both primary and final isotones of $N = 126$ can be seen to hold the large production tendency for the MNT reaction, which is consistent with the experiment. The DNS

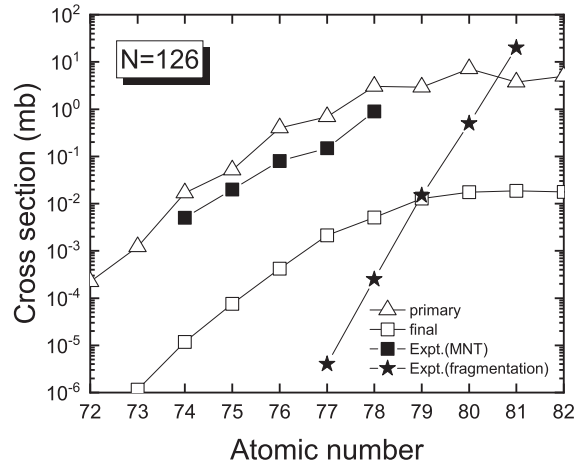

FIG. 7. (a) Production cross sections of the $N = 126$ isotones as a function of the atomic number. Calculations of primary and final products in the ^{136}Xe + ^{198}Pt reaction with $E_{\mathrm{c.m.}} = 643$ MeV are denoted by opened diamonds and squares, respectively. The filled squares are from the MNT experiment [9], while the filled stars are from the fragmentation experiment of ^{208}Pb(1 GeV/nucleon) + Be [3], for comparison.

calculation supports the MNT reaction as a more promising way to produce neutron-rich isotopes of interest.

IV. SUMMARY

In conclusion, influences of dynamical deformation on the PES and the mass distribution of the MNT reaction are investigated in the framework of the DNS concept. The distribution of primary and final products in MNT reactions ^{136}Xe + ^{198}Pt, ^{136}Xe + ^{208}Pb at collision energies above the Coulomb barrier are roughly in agreement with experiment, respectively, especially in the distribution trend. Orientation effect on the final isotope distributions of the reaction ^{136}Xe + ^{198}Pt at the collision energy about 1.55 times the Coulomb barrier is investigated. In such a collision energy, it is possible to have certain distribution probabilities of DNS configuration with all possible orientations at the exit point. Three different extreme cases are assumed to discuss the orientation effect for simplicity. The calculated behavior of the final products distribution reveals that the side-to-side orientation has an advantage in contributing to the production of neutron-rich nuclei of interest, owing to the small excitation of primary products at the exit channel. The present study reveals the applicability of the DNS in describing the MNT reaction which may be a promising way to produce new neutron-rich nuclei.

ACKNOWLEDGMENTS

The work is supported by the Natural Science Foundation of China (Grants No. 11475115, No. 11675066, No. 11847235, No. 11705118, and No. 11665019).

[1] H. Grawe, K. Langanke, and G. Martínez-Pinedo, Nuclear structure and astrophysics, Rep. Prog. Phys. **70**, 1525 (2007).
[2] G. Lorusso *et al.*, β-Decay Half-Lives of 110 Neutron-Rich Nuclei Across the $N = 82$ Shell Gap: Implications for the Mechanism and Universality of the Astrophysical *r* Process, Phys. Rev. Lett. **114**, 192501 (2015).
[3] T. Kurtukian-Nieto, J. Benlliure, K.-H. Schmidt, L. Audouin, F. Becker, B. Blank, E. Casarejos, F. Farget, M. Fernández-Ordóñez, J. Giovinazzo, D. Henzlova, B. Jurado, J. Pereira, and O. Yordanov, Production cross sections of heavy neutron-rich nuclei approaching the nucleosynthesis *r*-process path around $A = 195$, Phys. Rev. C **89**, 024616 (2014).
[4] J. Kurcewicz, F. Farinon, H. Geissel, and S. Pietri, Discovery and cross-section measurement of neutron-rich isotopes in the element range from neodymium to platinum with the FRS, Phys. Lett. B **717**, 371 (2012).
[5] H. Alvarez-Pol, J. Benlliure, E. Casarejos, L. Audouin, D. Cortina-Gil, T. Enqvist, B. Fernndez-Domnguez, A. R. Junghans, B. Jurado, P. Napolitani, J. Pereira, F. Rejmund, K.-H. Schmidt, and O. Yordanov, Production of new neutron-rich isotopes of heavy elements in fragmentation reactions of ^{238}U projectiles at 1*A* GeV, Phys. Rev. C **82**, 041602(R) (2010).
[6] E. M. Kozulin, E. Vardaci, G. N. Knyazheva, A. A. Bogachev, S. N. Dmitriev, I. M. Itkis, M. G. Itkis, A. G. Knyazev, T. A. Loktev, K. V. Novikov, E. A. Razinkov, O. V. Rudakov, S. V. Smirnov, W. Trzaska, and V. I. Zagrebaev, Mass distributions of the system ^{136}Xe + ^{208}Pb at laboratory energies around the coulomb barrier: A candidate reaction for the production of neutron-rich nuclei at $N = 126$, Phys. Rev. C **86**, 044611 (2012).
[7] E. M. Kozulin, V. I. Zagrebaev, G. N. Knyazheva, I. M. Itkis, K. V. Novikov, M. G. Itkis, S. N. Dmitriev, I. M. Harca, A. E. Bondarchenko, A. V. Karpov, V. V. Saiko, and E. Vardaci, Inverse quasifission in the reactions ^{156,160}Gd + ^{186}W, Phys. Rev. C **96**, 064621 (2017).
[8] J. S. Barrett, W. Loveland, R. Yanez, S. Zhu, A. D. Ayangeakaa, M. P. Carpenter, J. P. Greene, R. V. F. Janssens, T. Lauritsen, E. A. McCutchan, A. A. Sonzogni, C. J. Chiara, J. L. Harker, and W. B. Walters, ^{136}Xe + ^{208}Pb reaction: A test of models of multinucleon transfer reactions, Phys. Rev. C **91**, 064615 (2015).
[9] Y. X. Watanabe, Y. H. Kim, S. C. Jeong, Y. Hirayama, N. Imai, H. Ishiyama, H. S. Jung, H. Miyatake, S. Choi, J. S. Song, E. Clement, G. de France, A. Navin, M. Rejmund, C. Schmitt, G. Pollarolo, L. Corradi, E. Fioretto, D. Montanari, M. Niikura, D. Suzuki, H. Nishibata, and J. Takatsu, Pathway for the Production of Neutron-Rich Isotopes Around the $N = 126$ Shell Closure, Phys. Rev. Lett. **115**, 172503 (2015).
[10] L. Corradi, G. Pollarolo, and S. Szilner, Multinucleon transfer processes in heavy-ion reactions, J. Phys. G **36**, 113101 (2009).
[11] J. Kratz, W. Loveland, and K. Moody, Syntheses of transuranium isotopes with atomic numbers $Z \leqslant 103$ in multi-nucleon transfer reactions, Nucl. Phys. A **944**, 117 (2015).
[12] S. Lunardi *et al.*, Spectroscopy of neutron-rich Fe isotopes populated in the ^{64}Ni + ^{238}U reaction, Phys. Rev. C **76**, 034303 (2007).
[13] J. J. Valiente-Dobón *et al.*, Lifetime Measurements of the Neutron-Rich $N = 30$ Isotones ^{50}Ca and ^{51}Sc: Orbital Dependence of Effective Charges in the *f p* shell, Phys. Rev. Lett. **102**, 242502 (2009).
[14] S. Szilner *et al.*, Interplay between single-particle and collective excitations in argon isotopes populated by transfer reactions, Phys. Rev. C **84**, 014325 (2011).
[15] A. Winther, Grazing reactions in collisions between heavy nuclei, Nucl. Phys. A **572**, 191 (1994).
[16] A. Winther, Dissipation, polarization and fluctuation in grazing heavy-ion collisions and the boundary to the chaotic regime, Nucl. Phys. A **594**, 203 (1995).
[17] http://personalpages.to.infn.it/~nanni/grazing/.
[18] V. Zagrebaev and W. Greiner, Production of New Heavy Isotopes in Low-Energy Multinucleon Transfer Reactions, Phys. Rev. Lett. **101**, 122701 (2008).
[19] V. I. Zagrebaev and W. Greiner, Production of heavy trans-target nuclei in multinucleon transfer reactions, Phys. Rev. C **87**, 034608 (2013).
[20] A. V. Karpov and V. V. Saiko, Modeling near-barrier collisions of heavy ions based on a langevin-type approach, Phys. Rev. C **96**, 024618 (2017).
[21] V. V. Saiko and A. V. Karpov, Analysis of multinucleon transfer reactions with spherical and statically deformed nuclei using a Langevin-type approach, Phys. Rev. C **99**, 014613 (2019).

[22] N. V. Antonenko, E. A. Cherepanov, A. K. Nasirov, V. B. Permjakov, and V. V. Volkov, Competition between complete fusion and quasi-fission in reactions between massive nuclei. The fusion barrier, Phys. Lett. B **319**, 425 (1993).

[23] G. G. Adamian, N. V. Antonenko, V. V. Sargsyan, and W. Scheid, Possibility of production of neutron-rich Zn and Ge isotopes in multinucleon transfer reactions at low energies, Phys. Rev. C **81**, 024604 (2010).

[24] A. Diaz-Torres, G. G. Adamian, N. V. Antonenko, and W. Scheid, Melting or nucleon transfer in fusion of heavy nuclei?, Phys. Lett. B **481**, 228 (2000).

[25] Z. Q. Feng, Production of neutron-rich isotopes around $N = 126$ in multinucleon transfer reactions, Phys. Rev. C **95**, 024615 (2017).

[26] L. Zhu *et al.*, Theoretical study on production of heavy neutron-rich isotopes around the $N = 126$ shell closure in radioactive beam induced transfer reactions, Phys. Lett. B **767**, 437 (2017).

[27] M. Huang, Z. Zhang, Z. Gan, X. Zhou, J. Li, and W. Scheid, Dynamical deformation in heavy ion collisions and formation of superheavy nuclei, Phys. Rev. C **84**, 064619 (2011).

[28] X. J. Bao *et al.*, Influence of neutron excess of projectile on multinucleon transfer reactions, Phys. Lett. B **785**, 221 (2018).

[29] S. Szilner, L. Corradi, G. Pollarolo, S. Beghini, B. R. Behera, E. Fioretto, A. Gadea, F. Haas, A. Latina, G. Montagnoli, F. Scarlassara, A. M. Stefanini, M. Trotta, A. M. Vinodkumar, and Y. Wu, Multinucleon transfer processes in ^{40}Ca + ^{208}Pb, Phys. Rev. C **71**, 044610 (2005).

[30] L. Corradi, A. M. Stefanini, D. Ackermann, S. Beghini, G. Montagnoli, C. Petrache, F. Scarlassara, C. H. Dasso, G. Pollarolo, and A. Winther, Multinucleon transfer reactions in ^{32}S+^{208}Pb close to the Coulomb barrier, Phys. Rev. C **49**, R2875 (1994).

[31] K. Sekizawa and K. Yabana, Time-dependent Hartree-Fock calculations for multinucleon transfer and quasifission processes in the ^{64}Ni + ^{238}U reaction, Phys. Rev. C **93**, 054616 (2016).

[32] K. Sekizawa, TDHF theory and its extensions for the multinucleon transfer reaction: A mini review, Frontiers in Physics **7**, 20 (2019).

[33] C. Simenel and A. Umar, Heavy-ion collisions and fission dynamics with the time-dependent Hartree-Fock theory and its extensions, Prog. Part. Nucl. Phys. **103**, 19 (2018).

[34] Z. Wu and L. Guo, Microscopic studies of production cross sections in multinucleon transfer reaction ^{58}Ni + ^{124}Sn, Phys. Rev. C **100**, 014612 (2019).

[35] X. Jiang and N. Wang, Production mechanism of neutron-rich nuclei around $N = 126$ in the multi-nucleon transfer reaction ^{132}Sn + ^{208}Pb, Chin. Phys. C **42**, 104105 (2018).

[36] K. Sekizawa and K. Hagino, Time-dependent Hartree-Fock plus Langevin approach for hot fusion reactions to synthesize the $Z = 120$ superheavy element, Phys. Rev. C **99**, 051602(R) (2019).

[37] N. Wang and L. Guo, New neutron-rich isotope production in ^{154}Sm + ^{160}Gd, Phys. Lett. B **760**, 236 (2016).

[38] N. Wang, L. Ou, Y. Zhang, and Z. Li, Microscopic dynamics simulations of heavy-ion fusion reactions induced by neutron-rich nuclei, Phys. Rev. C **89**, 064601 (2014).

[39] K. Zhao, Z. Li, N. Wang, Y. Zhang, Q. Li, Y. Wang, and X. Wu, Production mechanism of neutron-rich transuranium nuclei in ^{238}U + ^{238}U collisions at near-barrier energies, Phys. Rev. C **92**, 024613 (2015).

[40] C. Li *et al.*, Production mechanism of new neutron-rich heavy nuclei in the ^{136}Xe + ^{198}Pt reaction, Phys. Lett. B **776**, 278 (2018).

[41] S. Ayik, A stochastic mean-field approach for nuclear dynamics, Phys. Lett. B **658**, 174 (2008).

[42] S. Ayik, B. Yilmaz, O. Yilmaz and A. S. Umar, Quantal diffusion approach for multinucleon transfers in Xe + Pb collisions, Phys. Rev. C **100**, 014609 (2019).

[43] S. Ayik, B. Yilmaz, O. Yilmaz, A. S. Umar, and G. Turan, Multinucleon transfer in central collisions of ^{238}U + ^{238}U, Phys. Rev. C **96**, 024611 (2017).

[44] B. Yilmaz, S. Ayik, O. Yilmaz, and A. S. Umar, Multinucleon transfer in ^{58}Ni + ^{60}Ni and ^{60}Ni + ^{60}Ni in a stochastic mean-field approach, Phys. Rev. C **98**, 034604 (2018).

[45] S. Ayik, B. Yilmaz, O. Yilmaz, and A. S. Umar, Quantal diffusion description of multinucleon transfers in heavy-ion collisions, Phys. Rev. C **97**, 054618 (2018).

[46] S. Ayik, O. Yilmaz, B. Yilmaz, and A. S. Umar, Heavy-isotope production in ^{136}Xe + ^{208}Pb collisions at $E_{\mathrm{c.m.}} = 514$ MeV, Phys. Rev. C **100**, 044614 (2019).

[47] M.-H. Mun, G. G. Adamian, N. V. Antonenko, Y. Oh, and Y. Kim, Toward neutron-rich nuclei via transfer reactions with stable and radioactive beams, Phys. Rev. C **91**, 054610 (2015).

[48] K. Zhao *et al.*, Production of unknown neutron-rich isotopes in ^{238}U + ^{238}U collisions at near-barrier energy, Phys. Rev. C **94**, 024601 (2016).

[49] E. M. Kozulin *et al.*, Shell effects in fission, quasifission and multinucleon transfer reaction, J. Phys.: Conf. Ser. **515**, 012010 (2014).

[50] S. Szilner *et al.*, Multinucleon transfer reactions in closed-shell nuclei, Phys. Rev. C **76**, 024604 (2007).

[51] E. M. Kozulin, G. N. Knyazheva, S. N. Dmitriev, I. M. Itkis, M. G. Itkis, T. A. Loktev, K. V. Novikov, A. N. Baranov, W. H. Trzaska, E. Vardaci, S. Heinz, O. Beliuskina, and S. V. Khlebnikov, Shell effects in damped collisions of ^{88}Sr with ^{176}Yb at the Coulomb barrier energy, Phys. Rev. C **89**, 014614 (2014).

[52] C. Li, C. A. T. Sokhna, X. Xu, J. Li, G. Zhang, B. Li, Z. Ge, and F.-S. Zhang, Isospin equilibration in multinucleon transfer reaction at near-barrier energies, Phys. Rev. C **99**, 034619 (2019).

[53] F. Niu, P.-H. Chen, Y.-F. Guo, C.-W. Ma, and Z.-Q. Feng, Effect of isospin diffusion on the production of neutron-rich nuclei in multinucleon transfer reactions, Phys. Rev. C **97**, 034609 (2018).

[54] W. Królas *et al.*, Dynamical deformation of nuclei in deep-inelastic collisions: A gamma coincidence study of ^{130}Te + 275 MeV ^{64}Ni and ^{208}Pb + 345 MeV ^{58}Ni heavy ion reactions, Nucl. Phys. A **832**, 170 (2010).

[55] W. Królas *et al.*, Gamma coincidence study of ^{208}Pb + 350 MeV ^{64}Ni collisions, Nucl. Phys. A **724**, 289 (2003).

[56] A. Nasirov *et al.*, The role of orientation of nucleus symmetry axis in fusion dynamics, Nucl. Phys. A **759**, 342 (2005).

[57] L. Yu *et al.*, Deformation relaxation in heavy-ion collisions, Phys. Lett. B **730**, 105 (2014).

[58] X. J. Bao, S. Q. Guo, H. F. Zhang, and J. Q. Li, Dynamics of complete and incomplete fusion in heavy ion collisions, Phys. Rev. C **97**, 024617 (2018).

[59] G. Wolschin and W. Nörenberg, Analysis of relaxation phenomena in heavy-ion collisions, Z. Phys. A **284**, 209 (1978).
[60] C. Riedel, G. Wolschin, and W. Nörenberg, Relaxation times in dissipative heavy-ion collisions, Z. Phys. A **290**, 47 (1979).
[61] J. Q. Li and G. Wolschin, Distribution of the dissipated angular momentum in heavy-ion collisions, Phys. Rev. C **27**, 590 (1983).
[62] S. Q. Guo, Y. Gao, J. Q. Li, and H. F. Zhang, Dynamical deformation in heavy ion reactions and the characteristics of quasifission products, Phys. Rev. C **96**, 044622 (2017).
[63] S. Ayik, B. Schürmann, and W. Nörenberg, Microscopic transport theory of heavy-ion collisions, Z. Phys. A **279**, 145 (1976).
[64] G. Chaudhuri and S. Mallik, Effect of liquid drop model parameters on nuclear liquid-gas phase transition, Phys. Rev. C **99**, 054602 (2019).
[65] N. Wang, M. Liu, and X. Wu, Modification of nuclear mass formula by considering isospin effects, Phys. Rev. C **81**, 044322 (2010).
[66] C. Y. Wong, Interaction Barrier in Charged-Particle Nuclear Reactions, Phys. Rev. Lett. **31**, 766 (1973).
[67] G. G. Adamian *et al.*, Effective nucleus-nucleus potential for calculation of potential energy of a dinuclear system, Int. J. Mod. Phys. E **05**, 191 (1996).
[68] Q. Li, W. Zuo, W. Li *et al.*, Deformation and orientation effects in the driving potential of the dinuclear model, Eur. Phys. J. A **24**, 223 (2005).
[69] R. J. Charity, Systematic description of evaporation spectra for light and heavy compound nuclei, Phys. Rev. C **82**, 014610 (2010).
[70] http://bitbucket.org/arekfu/gemini/src/master/.
[71] D. Mancusi, R. J. Charity, and J. Cugnon, Unified description of fission in fusion and spallation reactions, Phys. Rev. C **82**, 044610 (2010).
[72] L. Corradi, A. M. Vinodkumar, A. M. Stefanini *et al.*, Light and heavy transfer products in ^{58}Ni+^{208}Pb at the Coulomb barrier, Phys. Rev. C **66**, 024606 (2002).